PHYSICS

Dynamics of proximity-induced magnetism at cobalt/molecular interfaces

Jaka Strohsack[1,2], Andrei V. Shumilin[1,3], Hui Zhao[1], Gregor Jecl[1], Viktor V. Kabanov[1], Mattia Benini[4], Rajib K. Rakshit[4], Valentin A. Dediu[4], Matthew D. Rogers[5], Servet Ozdemir[5], Oscar Cespedes[5], Umut Parlak[6], Mirko Cinchetti[6], Tomaz Mertelj[1,7]*

Copyright © 2025 The Authors, some rights reserved; exclusive licensee American Association for the Advancement of Science. No claim to original U.S. Government Works. Distributed under a Creative Commons Attribution NonCommercial License 4.0 (CC BY-NC).

Interfacing ferromagnetic metals with organic molecules is a versatile strategy to control key parameters in magnetic and spintronic technologies. Hybridization between the metal's surface d orbitals and molecular p orbitals profoundly alters both the interfacial molecular layer and adjacent metal interface atomic layers, causing substantial changes in the magnetic properties of metal/molecule heterostructures. While magnetic modifications within the metallic layer are relatively well understood, the interfacial magnetism remains elusive. Using ultrafast time-resolved magneto-optical spectroscopy, we investigate the magnetic dynamics in such heterostructures and identify a distinct interfacial magnetic component that appears universal across various cobalt/molecule combinations. Our findings reveal a highly anisotropic magnetic layer localized at the interface, which has remained undetected in static measurements. This interfacial layer likely originates from strong chemical modifications in the cobalt surface induced by chemisorbed molecules. These results underscore the crucial role of molecular chemisorption in shaping interfacial magnetic properties, offering further opportunities for tuning functionalities in molecule-based spintronic devices.

INTRODUCTION

Hybridized interfaces between 3d ferromagnetic (FM) metals and organic molecules have attracted substantial attention due to their fundamental phenomena and promising functional properties (*1*). These interfaces have been extensively studied over the past decade (*2*–*12*), revealing substantial alterations in the magnetic behavior of thin FM films following the deposition of a single molecular layer (*3*, *4*). These changes are primarily attributed to the hybridization between the surface d orbitals of the FM metal and the p orbitals of the adsorbed molecules (*1*, *4*, *12*, *13*).

Most previous studies have focused on static magnetization properties (*2*–*5*, *7*, *8*, *10*–*12*, *14*), often reporting enhanced coercivity at low temperatures. It was also demonstrated that the magnetic hardening is accompanied by a transition to an unusual correlated FM glass state (*14*). While the enhanced coercivity can be understood in the frame of a phenomenological description, its relationship to microscopic magnetic parameters remains indirect (*14*). Furthermore, the frequently observed temperature dependence—where effects diminish at room temperature (*3*, *4*, *7*, *8*, *10*)—is not yet fully understood. In cobalt (Co)/buckminsterfullerene (C_{60}) systems, for example, this temperature behavior has been linked to a specific rotational transition of the C_{60} molecule (*7*), which does not apply to molecules with different geometries.

To advance our understanding, more direct and complementary data are needed, particularly for interfaces with molecules of diverse shapes. These data should probe microscopic quantities such as magnetic anisotropy and possible exchange bias. Time-resolved magneto-optical Kerr effect (TR-MOKE) spectroscopy is ideally suited for this purpose, as it enables spatially localized and broadband probing of magnetic dynamics (*15*). In particular, it can be used to map the effective anisotropy field of thin films, thereby revealing microscopic parameters of the magnetic free energy (*16*, *17*).

In this study, we present a systematic TR-MOKE investigation of several Co/molecule interfaces. We examine the effects of four molecular species with distinctly different geometries: the highly asymmetric tris(8-hydroxyquinoline)gallium (Gaq_3), the spherical C_{60}, and two nearly planar metal-phthalocyanines (MPcs; with M = Cu and Co). A detailed list of the studied heterostructures is shown in Fig. 1C. Using femtosecond laser pulses, we weakly perturb the equilibrium magnetization (*16*, *17*) and excite coherent spin waves, which we detect with time-delayed probe pulses, as schematically illustrated in Fig. 1A. To remain within the linear response regime and avoid nonlinear excitation of the molecular layers or nonequilibrium effects in the ferromagnet (*18*–*20*), we keep the laser perturbation rather weak.

By varying the external magnetic field, H, in a quasi-polar MOKE geometry, we map the effective anisotropy field, H_{eff}, over a range of out-of-plane magnetization angles, allowing us to extract the parameters of the effective magnetic free energy. Our measurements reveal a strong hardening of the spin-wave frequency upon cooling below ~200 K. The magnetic field–dependent spin-wave spectra indicate that the Co/molecule interface suppresses the effective easy-plane anisotropy of the Co film while also introducing a strong in-plane exchange-bias–like anisotropy. The corresponding effective bias field reaches values of $\mu_0 H_b = 0.6$ T at low temperatures. Notably, this behavior is consistent across all molecular species studied, regardless of their shape, and is attributed to the onset of a strongly anisotropic magnetic ordering at the hybridized interface below 170 to 200 K.

[1]Department of Complex Matter, Jozef Stefan Institute, Jamova 39, 1000 Ljubljana, Slovenia. [2]Faculty of Mathematics and Physics, University of Ljubljana, Jadranska 19, 1000 Ljubljana, Slovenia. [3]Instituto de Ciencia Molecular, Universitat de València, Catedrático José Beltrán 2, 46980 Paterna, Spain. [4]ISMN-CNR, Via Piero Gobetti 101, Bologna, Italy. [5]School of Physics and Astronomy, University of Leeds, Leeds LS2 9JT, UK. [6]Technische Universität Dortmund, Otto-Hahn-Straße 4, Dortmund, Germany. [7]Center of Excellence on Nanoscience and Nanotechnology Nanocenter (CENN Nanocenter), Jamova 39, 1000 Ljubljana, Slovenia.
*Corresponding author. Email: tomaz.mertelj@ijs.si

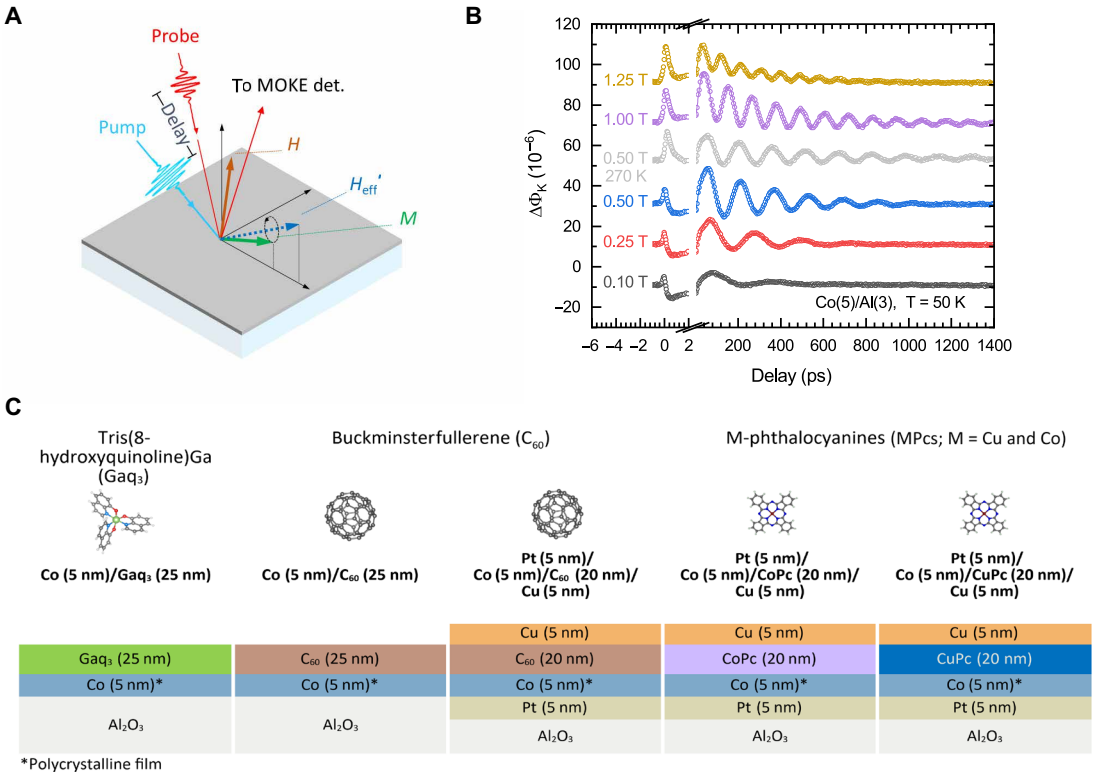

Fig. 1. Experimental setup and samples. (**A**) Schematics of the experimental geometry. (**B**) Transient magneto-optical Kerr rotation in a reference Co(5)/Al(3) sample at T = 50 K. A trace obtained at T = 270 K and $\mu_0 H = 0.5$ T (gray) is shown for comparison to emphasize weak T dependence. The lines correspond to the damped oscillator fit eq. S1 discussed in the main text. (**C**) Schematic representation of the studied heterostructures. det., detector.

RESULTS

In Fig. 2 (A and B), we show, as an example, the temperature- and magnetic field–dependent transient magneto-optical Kerr angle, $\Delta\Phi_K$, in the Pt(5)/Co(5)/CoPc(20)/Cu(5) heterostructure where numbers in parentheses correspond to the thickness of the layers given in nanometers. $\Delta\Phi_K$ is characterized by the presence of coherent oscillations that correspond to the spin waves (*16*, *17*). The comparison to the reference Co(5)/Al(3) heterostructure, where the Al layer is used to protect the Co film from oxidation, shows similar spin waves at room temperature. Upon cooling, the reference transients show only minor change (see Fig. 1B), while the Co/molecular heterostructures show hardening of the spin-wave frequency (Fig. 2, D and E), increased damping (Fig. 2F), and a $\Delta\Phi_K$ sign change below T = 170 K (Fig. 2A). Other samples from Fig. 1C show qualitatively similar behavior (see fig. S1). A similar hardening of the ferromagnetic resonance (FMR) frequency has also been reported in thicker Co/C_{60} heterostructures (*21*).

The spin-wave frequency is dependent on the external magnetic field, *H*, showing hysteretic behavior (see Fig. 3 and fig. S2). The hysteresis depends on the applied external magnetic field during cooling and exhibits training behavior. In the Pt(5)/Co(5)/C_{60}(20)/Cu(5) sample upon field cooling, for example, we initially observe a reversible monotonous magnetic-field frequency dependence down to the negative irreversibility field, $\mu_0 H_{ir-} = -0.7$ T ($\nu = 19$ GHz) (see Fig. 3A, point #37). In the subsequent loops (Fig. 3B), after some training, the frequency does not drop below $\nu = 20.5$ GHz anymore and shows an upturn with decreasing *H* around $\mu_0 H = -0.4$ T already. The hysteresis closing is asymmetric at $\mu_0 H_{c-} = -0.9$ T on the negative and $\mu_0 H_{c+} = -0.6$ T on the positive side, showing a field-offset behavior.

The zero-field cooling data show qualitatively similar hysteresis (see fig. S2), albeit with a smaller field offset, which was not studied in detail. Most of the data (Figs. 2E and 4A) were acquired upon zero-field cooling without reversing *H*. These scans showed mostly reversible behavior when sweeping *H* from a small to the largest field and back. Some additional scatter sometimes observed at low *H* can be attributed to the presence of the hysteresis.

The damping shows only a weak magnetic field dependence while increasing ~3 to 4 times with decreasing T below ~170 K (Fig. 2F). From the present data, it is not possible to distinguish the dissipation and dephasing contributions to the damping. As the molecular layer is disordered (*14*), the dominant contribution to the increase is tentatively attributed to dephasing. Comparing the low-T *H* dependence for different molecules, we observe qualitatively similar behavior with the low-*H* spin-wave frequency in the 20 to 30 GHz range, which is ~10 times larger than the room-T [as well as the Co(5)/Al(3) reference sample] value (Fig. 2E and 4A). The static magneto-optical Kerr angle, corresponding to the magnetization component perpendicular to the film, is shown in Fig. 2C. Within the experimental accuracy, the static Kerr angle does not show any T dependence or a clear hysteresis.

The low-*H* spin-wave frequency T dependence is summarized in Fig. 4 (B to D). The behavior is qualitatively similar in all studied heterostructures. The spin-wave frequency hardening with decreasing T sets in around T = 200 K with a more pronounced jump in the 150- to 170-K range (depending on the molecular species) concurrently

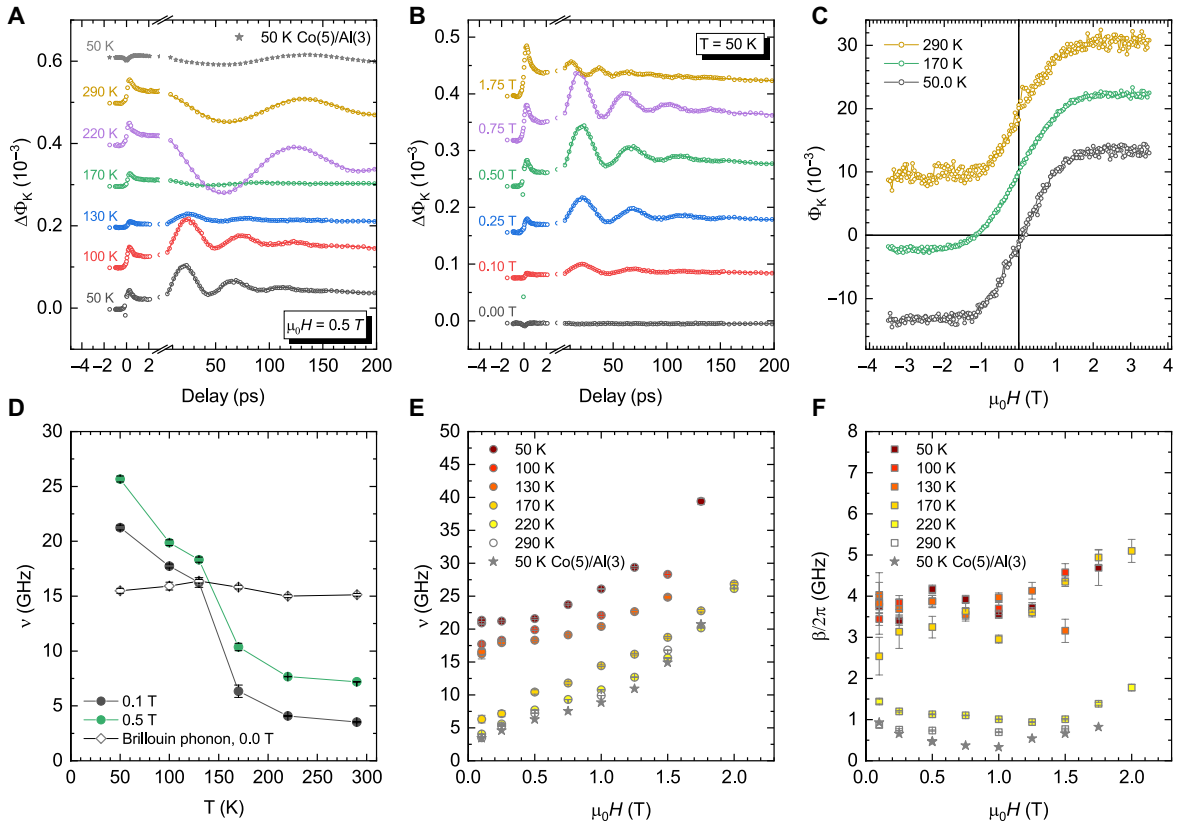

Fig. 2. Transient and static MOKE in Pt(5)/Co(5)/CoPc(20)/Cu(5) heterostructure. (**A**) Temperature dependence of MOKE transients at $\mu_0 H = 0.5$ T. (**B**) Magnetic field dependence of MOKE transients at T = 50 K. (**C**) The static Kerr rotation loops as a function of T. (**D**) The spin-wave frequency as a function of T. The open symbols correspond to the coherent Brillouin waves observed in transient reflectivity (see fig. S6). (**E**) The spin-wave frequency as a function of *H* at different T. (**F**) The spin-wave damping as a function of *H* at different T. The traces in (A) to (C) are vertically offset for clarity. The lines in (A) and (B) are damped oscillator fits (see eq. S1).

with the oscillation sign change. The effect does not depend notably on the details of the auxiliary heterostructure layers as indicated by the data from two different C_{60}-based heterostructures (Fig. 4D).

DISCUSSION

Origin of coherent spin waves

The reference Co(5)/Al(3) heterostructure *H* dependence of the spin-wave frequency can be successfully modeled (the fit line in Fig. 4A), assuming a homogeneous magnetization precession with an easy-plane anisotropy of $K_\perp M_0 = 1.1$ T, in the full T range [see Supplementary Text and (*22*)]. For simplicity, we merge both the shape and magnetocrystalline anisotropy contributions into $K_\perp$. At high T, the Co/molecule heterostructure spin-wave frequency *H* dependencies show similar behaviors as the Co(5)/Al(3) reference sample (see Fig. 2E). The high-T dynamic behavior, together with the static data (see Fig. 2C), is therefore consistent with the easy-plane anisotropy of $K_\perp M_0 = 1.1$ T, as in the Co(5)/Al(3) reference sample.

At low T, however, the spin-wave frequency *H* dependencies (Fig. 4A) appear incompatible with the simple easy-plane anisotropy model. Concurrently, the static Φ_K data (Fig. 2C) show a virtually T-independent behavior, suggesting the easy-plane–anisotropy model also at low T. The apparent dichotomy between the static and dynamic behavior could indicate that the observed coherent oscillations do not correspond to the uniform spin precession at low T but to a localized mode at the Co/molecule interface or a higher-order (*23*) standing spin-wave mode. This scenario is, however, very unlikely. The uniform mode (with a lower frequency) should always contribute to the response, but in the data, only one frequency component is observed in all samples (see fig. S1). Moreover, the optical penetration depth in Co at the probe wavelength of ~13 nm (*24*) is more than twice as large as the Co thickness. Any higher-order standing modes should have weak intensities in comparison to the uniform mode.

The uniform-mode bulk excitation is a consequence of a rapid change of the Co-film electronic and lattice temperatures (*17*) and cannot be directly suppressed by the interface interaction. The uniform-mode oscillation can therefore be suppressed only if the bulk and interface excitation contributions exactly cancel. This appears to happen around T = 170 K, where the hardening sets in and the signal vanishes (see Fig. 5). It is, however, extremely unlikely that both contributions would remain exactly balanced in the broad range of T below T = 170 K in all studied samples.

It is also unlikely that the interfacial magnetization would be pinned (*23*) because of the high exchange coupling and the small thickness of the Co film. The mean-field Weiss molecular field is estimated to be $\mu_0 H_W = 1000$ T in Co (*25*). The fundamental standing spin-wave mode is therefore expected to be negligibly nonuniform. As a result, the observed spin-wave oscillations correspond to the bulk Co-film dynamics, with a high degree of certainty. We can therefore discuss the magnetization precession as being uniform

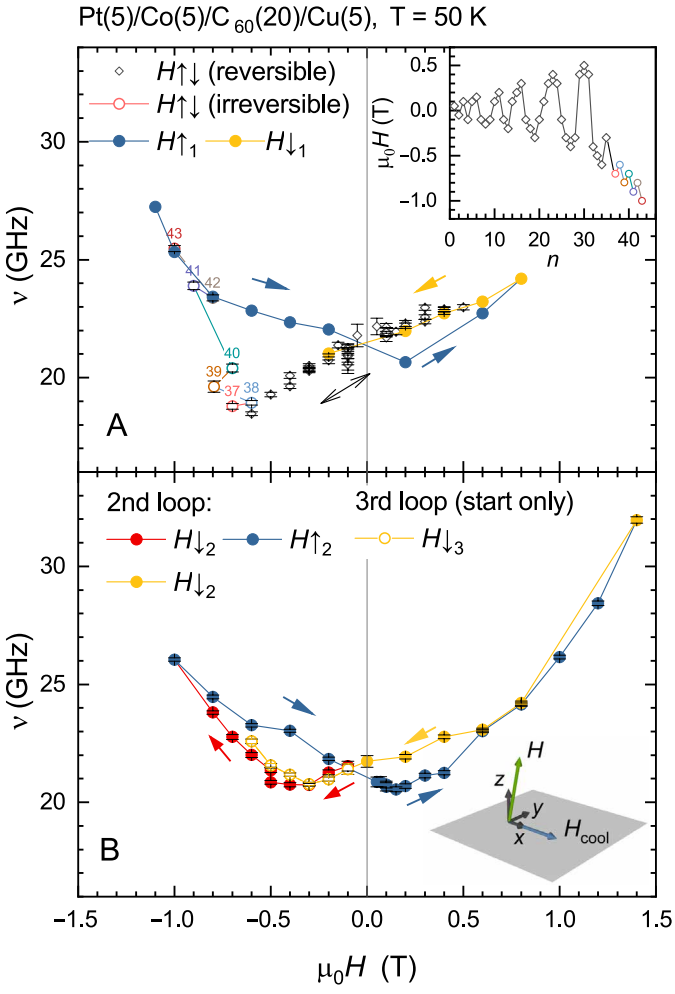

Fig. 3. Magnetic field dependence of the spin-wave frequency in the field-cooled (in-plane; u_0H_{cool} = 5 T) Pt(5)/Co(5)/C_{60}(20)/Cu(5) heterostructure. (**A**) The initial-branch reversible region (open diamonds) and the first irreversible loop. The initial oscillating magnetic-field sequence, corresponding to the open symbols, is shown in the inset. The full symbols represent subsequent measurements where the magnetic field was swept monotonously from −1 to 0.8 T and back to −0.2 T. The number labels indicate the sequential measurements to emphasize the nonmonotonous field sequence in the first part of the loop. (**B**) The second and the beginning of the third loop measured after the first loop. The magnetic field was swept in a monotonous manner: –0.1 T → –1 T → 1.4 T → –0.6 T.

along the thickness of the Co film, where the interface-induced anisotropy and/or exchange bias can be treated as a (properly renormalized) volume contribution.

Magnetic field dependence modeling

To understand the static behavior in an in-plane external magnetic field, they previously assumed (*14*) that the effect of molecules at the interface is an induced effective in-plane magnetic-anisotropy free-energy term, $K_{\parallel}\left(\mathbf{M}\cdot\mathbf{e}_R\right)^2/2$, where $K_{\parallel} \ll K_{\perp}$ and $K_{\parallel}M_0 = 0.1$ T, with a random but spatially correlated in-plane vector $\mathbf{e}_R$. Although such an anisotropy can lead to a quite unusual FM glass state for small external magnetic fields and explain the static measurements in an in-plane magnetic field (*14*), it cannot describe the observed spin-wave frequency magnitudes. At small external fields, where the magnetization lies in the heterostructure plane, the spin-wave frequency of ~25 GHz (Fig. 4A) corresponds to an in-plane effective field, $\mu_0H_{\parallel\text{eff}} = 0.9$ T. This value is much larger than expected from the static in-plane model parameters (*14*), where (*26*) $\mu_0H_{\parallel\text{eff}} = M_0\sqrt{K_{\parallel}\left(K_{\parallel}+K_{\perp}\right)} = 0.35$ T could be estimated from $K_{\parallel}M_0 = 0.1$ T and $K_{\perp}M_0 = 1.1$ T.

The increase of the spin-wave frequency in weak external fields could also be a consequence of the laterally inhomogeneous FM glass state (*14*); however, the low-T increase [with respect to the Co(5)/Al(3) reference] persists in the uniformly magnetized saturated magnetic state at large external magnetic fields. At $\mu_0H = 2$ T, for example, the precession frequency of ~40 GHz corresponds to an out-of-plane effective field of $\mu_0H_{\perp\text{eff}} = 1.5$ T, while a substantially smaller $\mu_0H_{\perp\text{eff}} = 1$ T is inferred (dominated by the easy-plane anisotropy) for the case of the Co(5)/Al(3) reference sample at the same external field.

To model the magnetic field dependence on equal footing through the full H range, we therefore, at first, neglect the low-H lateral inhomogeneity. The large low-H frequency suggests the presence of a rather strong in-plane anisotropy; however, this anisotropy leads to the spin-wave frequency H dependence that is incompatible with the observed behavior (see Fig. 6, fig. S7, and Supplementary Text). Alternatively, the strong in-plane effective field can be attributed to an exchange bias (*5*, *7*, *11*) present at the Co/molecule interface. As shown in Fig. 6, it turns out that an addition of the in-plane exchange-bias–like free-energy term to the easy-plane–anisotropy model (see eq. S4) fairly reproduces both the dynamic and the out-of-plane static data, with an effective in-plane exchange-bias field of $\mu_0H_b = 0.6$ T and a reduced (with respect to the high-T behavior) effective easy-plane anisotropy of $K_{\perp}M_0 = 0.5$ T. Here, we take into account the zero-field cooling so we average over a random in-plane exchange-bias direction distribution.

Our data therefore suggest a picture where the presence of the Co/molecule interface induces rather strong modifications to the interfacial Co layer(s) in the form akin to an in-plane exchange bias. While the molecular-induced exchange-bias behavior has been observed previously (*5*, *9*, *27*), it might not be intrinsic (*11*). In particular, it has not been observed in the samples studied in this work [see Supplementary Text and (*3*, *10*, *14*)]. Moreover, the static in-plane magnetic behavior suggests a correlated random anisotropy (CRA) in the absence of any exchange-bias term (*14*). The above homogeneous model with a static exchange bias therefore appears inconsistent with the static in-plane behavior.

While the absence of a major static in-plane exchange-bias H shift can be attributed to a random in-plane distribution of the H_b directions, the assumed fixed H_b cannot be substantiated. The effective bulk exchange bias of $\mu_0H_b = 0.6$ T corresponds to the interface exchange field of the order of ~10 T. To realize a fixed exchange field of such a magnitude, the proximity of a bulk hard (anti)ferromagnet would be necessary. As the molecules a few layers away from the Co interface are unlikely to support any magnetic order, an interfacial magnetic state providing the exchange-bias–like free-energy term cannot be thick and bulk like.

Advanced model

There is, however, a possibility that the hybridization of the interface Co layer with molecules leads to the formation of a strongly anisotropic molecular-magnet–like interface magnetism. For example,

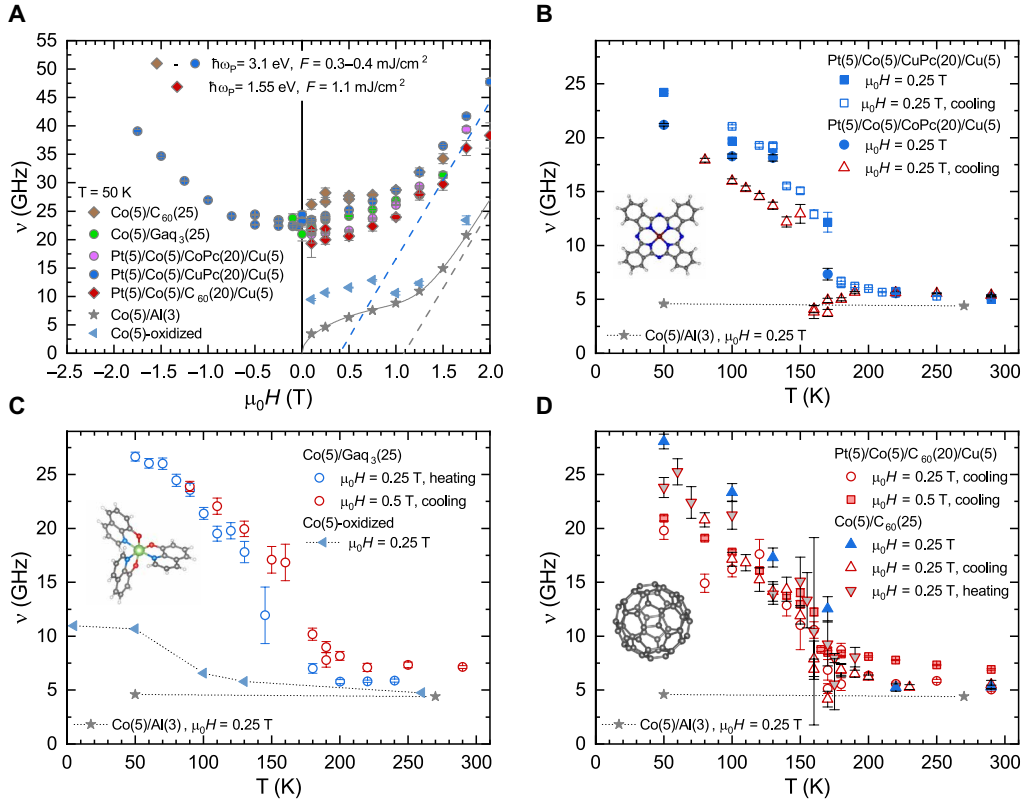

Fig. 4. The spin-wave frequency as a function of *H* and T in different heterostructures. (**A**) The frequency as a function of external magnetic field at T = 50 K in all studied samples upon zero-field cooling. The continuous gray line is the uniform-precession easy-plane fit (see eq. S2) to the reference Co(5)/Al(3) sample data. The dashed lines indicate the large-*H* asymptotics. (**B**) The frequency as a function of temperature at a constant external magnetic field in samples with CoPc and CuPc. (**C**) The frequency as a function of temperature at a constant external magnetic field in the sample with Gaq_3. (**D**) The frequency as a function of temperature at a constant external magnetic field in samples with C_{60}. The full single color symbols in (C) to (D) correspond to the data points obtained from the zero-field–cooling isothermal *H* scans at different T, while the nonuniform symbols correspond to the constant-*H* temperature scans. The blue symbols correspond to $\hbar\omega_p = 3.1$ eV and $F = 0.3$ to 0.4 mJ/cm^2, while the symbols with a red border correspond to $\hbar\omega_p = 1.55$ eV and $F = 1.1$ mJ/cm^2.

the high-spin Co(II) in low-symmetry organic complexes shows unquenched orbital momentum (*28*, *29*) with possibly large magnetic anisotropy up to several mega–electron volts per Co ion. A strong covalent bonding of the surface Co with the molecules combined with charge transfer might result in a similar magnetic anisotropy. To check whether such a molecular-magnet–like interface magnetism hypothesis can consistently explain the static in-plane and out-of-plane behavior together with the dynamical response, we extended the previously studied CRA model (*14*) by including an interfacial magnetic layer (IML) that is exchange coupled (J) to the bulk Co film. The correlated random in-plane anisotropy (K_{hy}) is assumed to act on the IML only (see Supplementary Text and inset to Fig. 7A). Furthermore, we assume that the Néel relaxation time is much faster than the spin-wave frequency so the local IML magnetization always follows the local IML effective field and is not blocked. As shown in Supplementary Text, the IML effective field is always large enough to keep the IML magnetization saturated. If the exchange coupling, J, is very large, then the IML magnetization, **m**, always follows the bulk Co-film magnetization, **M**, and the model becomes equivalent to the original CRA model. On the other hand, when the effective exchange field in the IML, $\mathrm{H}_{m,e} = J\mathbf{M}/\mu_0 M_0 m_0$, is comparable to the local anisotropy field, $H_{m,a} = K_{hy} m/\mu_0$, the IML magnetization acquires a finite angle with respect to **M**, resulting in an effective pseudo–exchange-bias (PEB) free-energy term, which is similar to an exchange-bias term (see eq. S10). (To describe the data in the full *H* range using the exchange-bias term, one would need to assume that the exchange-bias field is not blocked and reverses when the Co-film magnetization is reversed.)

As shown in Fig. 7, the behavior of such PEB-CRA model qualitatively matches all the in-plane and the out-of-plane static data, as well as the magnetic dynamics data. Comparing the theoretical spin-wave frequency hysteresis (Fig. 7A) with the Pt(5)/Co(5)/CuPc(20)/Cu(5) heterostructure data, the main discrepancy is the magnitude of the splitting between the lower and upper hysteresis branches. In the data, this splitting also varies with molecular species (see Fig. 3). Because, in addition to the model parameters and T, the hysteresis can be also affected by extrinsic effects such as grain boundaries and the laser excitation during measurement, we believe that the discrepancy is not essential.

The PEB-CRA model is also qualitatively consistent with the in-plane field-cooled dynamical hysteresis data (Fig. 3). However, similar to the low-T static in-plane hysteresis data upon field cooling [see (*7*) and fig. S9], strong training effects are observed during the initial out-of-plane magnetization saturation, and the subsequent hysteresis loops show a magnetic-field offset of ~0.1 to 0.2 T. While some training effects are observed in the simulations, the magnetic-field offset is

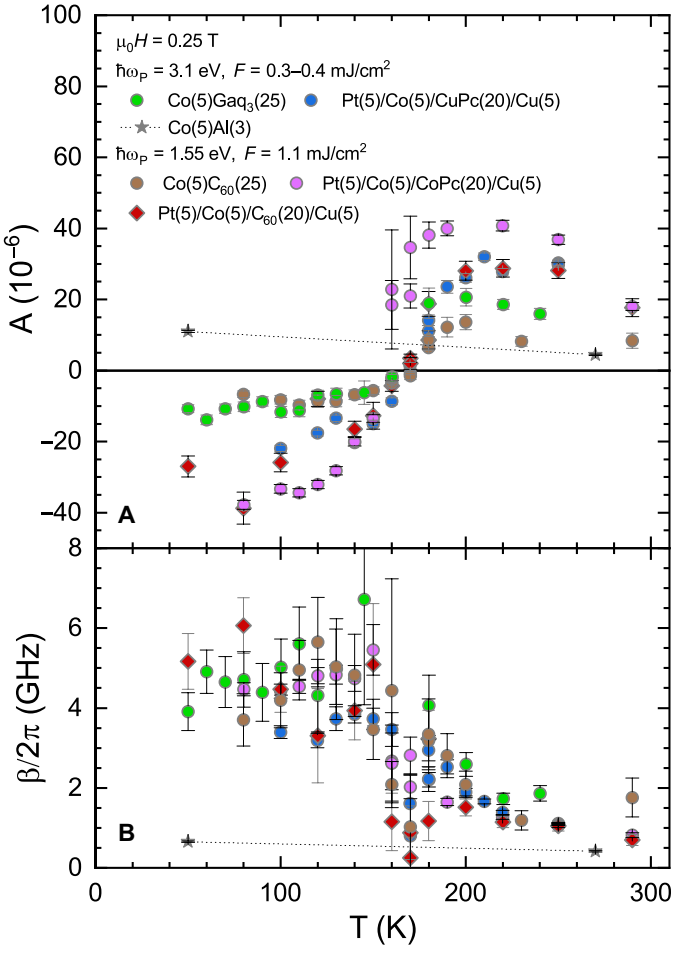

Fig. 5. Oscillation amplitude and damping as a function of T. Comparison of (**A**) the initial oscillation amplitude and (**B**) damping as a function of T in different heterostructures at $\mu_0 H = 0.25$ T.

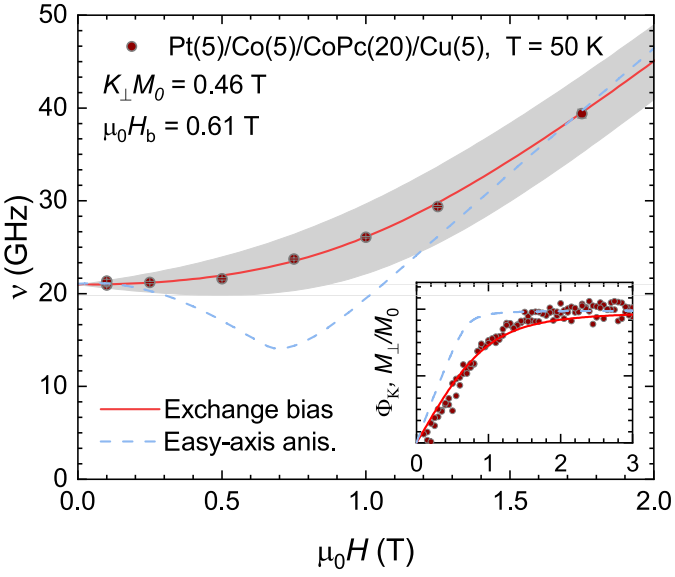

Fig. 6. Comparison of the exchange-bias model (eq. S4) spin-wave frequency to the data. The static out-of-plane response is shown in the inset. The full lines correspond to the average over a random in-plane exchange-bias direction distribution, while the gray band corresponds to the spread of frequencies across the distribution. The dashed line corresponds to the in-plane easy-axis model (eq. S3). anis., anisotropy.

forbidden by the symmetry. The presence of the magnetic-field offset in the field-cooling experiment therefore cannot be explained by the PEB-CRA model. As the magnetic field is nearly perpendicular to the heterostructure plane and the in-plane magnetic-field component in Fig. 3 did not exceed ~0.1 T, which is comparable to the in-plane coercivity (*14*), it is possible that the in-plane magnetization component in all grains was not fully reversed, and the experimental data correspond to a minor loop. This is very likely, as the presence of the low-T training effects indicates that the IML becomes partially blocked below T = 50 K. A partial IML blocking implies that the model is not strictly consistent at low T. However, the IML effective field is rather large and can overcome blocking in most of the IML layer even at low T.

Analysis of possible microscopic mechanisms behind frequency hardening

The data indicate that the general molecular shape does not strongly influence the molecule-induced PEB and the characteristic T scale. This could indicate that the interface is possibly oxidized as proposed recently (*11*). To check for oxidation, we also performed transient MOKE experiments in a thin film sample consisting of naturally oxidized 5-nm-thick Co. The presence of antiferromagnetic CoO_x at the surface also resulted in low-T spin-wave frequency hardening. The degree of hardening ($\nu = 10$ GHz at $\mu_0 H = 0$ T) is, however, substantially smaller with completely different T and H dependencies. A sharp, T-dependent, metamagnetic transition was observed around $\mu_0 H = 0.8$ T (at T = 50 K), which will be discussed in detail elsewhere (see Fig. 4, A and C, and fig. S5). The observed effects in the Co/molecule heterostructures can therefore be reliably attributed to the molecular chemisorption to the Co-film surface, although the possible role of oxygen contamination in the chemisorption remains unclear (*11*).

Empirically, the common feature of all the investigated molecules is the presence of aromatic rings that are predicted to hybridize with Co (*8*, *13*, *30*) via their π orbitals. In the case of Gaq_3 and C_{60}, the molecular geometry is such that only part of the rings is close enough to the interface to hybridize, while, in the case of MPc, all rings can hybridize. The surface density of the hybridized rings is therefore expected to be different for different molecules. The absence of large differences in the molecule-induced spin-wave frequency hardening and the onset T for different molecules suggests that the effect might be saturated beyond some critical hybridized Co-atom surface density; however, further studies are necessary to prove the hypothesis.

While strong interfacial modification is also experimentally hinted by the decrease of the saturated magnetic moment, up to ~15% upon covering a 5-nm-thick Co film with 20 nm of C_{60} (*3*, *8*), the ab-initio calculations (*8*, *12*, *13*, *30*) generally do not predict such strong effects. Here, we should take into account that our data suggest that the interfacial magnetic state should involve a correlated state possibly distributed laterally across several molecules, while the ab-initio calculations are usually limited to well-separated independent molecules and might miss the longer-range correlation effects. A related modification of a few-monolayer-thick Co-film

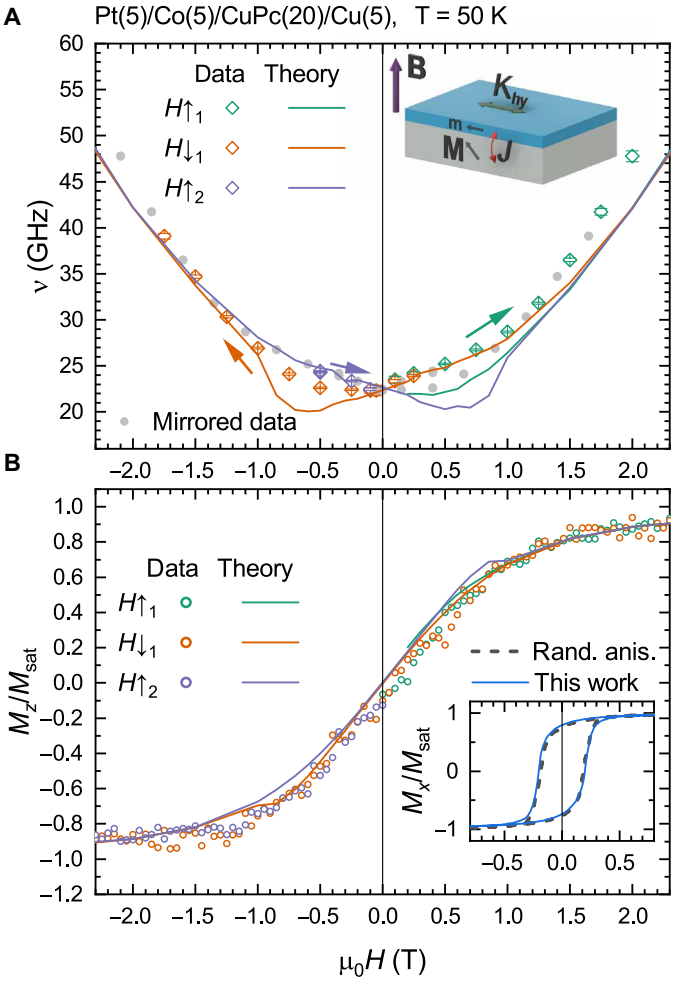

Fig. 7. Comparison of the PEB random-anisotropy model to the experimental data. (**A**) The spin-wave frequency hysteresis after zero-field cooling in the CuPc-based heterostructure compared to the model. The inset is a graphical illustration of the model. (**B**) The static out-of-plane response data compared to the model. The inset is a comparison of the theoretical in-plane hysteresis calculated with the random-anisotropy model (*14*) and the PEM random-anisotropy model. The parameters (eq. S11) for the simulated curves are $K_\perp M_0 = 0.6$ T, $K_{hy} m_0 = 14.6$ T, $J / m_0 = 18.3$ T, and $dM_0 / m_0 = 12$, corresponding to $\alpha = 1.2$ and $K_R M_0 = 0.61$ T. The correlation length is $r_c = 5.5\xi_c$ with ξ_c being the Co exchange length. Rand., random.

anisotropy upon covering with a graphene monolayer reported recently (*31*) also suggests that a formation of correlated C—Co bond arrays might be necessary to achieve the effect. The characteristic onset T = 200 K, associated with the spin-wave hardening effect, could therefore be connected with the enhancement of the correlation effects, leading to the interface magnetic ordering.

Conclusions and outlook

We systematically investigated the influence of Co/molecular interfaces on the magnetization dynamics of 5-nm-thick Co films using TR-MOKE spectroscopy. Despite the pronounced differences in molecular geometry—from spherical to planar and asymmetric structures—all studied molecules induced a substantial hardening of the spin-wave frequency below ~200 K. This consistency across diverse molecular systems points to a common interfacial mechanism. One plausible unifying feature is the presence of aromatic rings, which are known to hybridize effectively with Co d orbitals. While the specific role of aromaticity remains an open question and cannot be conclusively established within the scope of this work, our findings suggest that such hybridization plays a central role in modifying the interfacial magnetic properties. Further comparative studies involving nonaromatic molecules would be necessary to isolate this effect.

The observed hardening of the spin-wave frequency in zero external field indicates the emergence of a substantial in-plane effective field ($\mu_0 H_{\parallel \mathrm{eff}} = 0.9$ T) originating from the Co/molecule interface. Field-dependent measurements of both static and dynamic magnetizations reveal that this field is associated with a spatially correlated, random in-plane PEB. Unlike the conventional exchange bias, this effect reverses with the magnetization of the adjacent Co layer, indicating that it stems from a distinct anisotropic IML that forms below ~200 K and is confined to the interfacial region. This IML is likely a consequence of strong chemical modification of the Co surface through chemisorption of the molecular overlayer. Previous studies have shown that such chemisorption can lead to profound restructuring of the magnetic environment extending several nanometers into the metal layer, but the presence of a distinct and additional interface component has been revealed in this work through ultrafast magnetization dynamics.

Our results demonstrate that hybridization with molecular layers can strongly influence surface magnetism without compromising structural integrity—an encouraging sign for the integration of such interfaces into existing device fabrication processes. The robustness and reproducibility of the observed PEB and highly anisotropic magnetic behavior at low temperatures suggest that hybrid Co/molecule interfaces offer a promising platform for further exploration. In particular, they open up opportunities for tuning spin-dependent phenomena such as magnetic switching fields, spin-wave propagation characteristics, and spin pumping efficiency—key parameters in next-generation spintronic devices. These findings highlight the potential of molecular hybridization as a powerful tool for tailoring interfacial magnetic properties. Continued exploration of such interfaces, including systematic variation of molecular structure and adsorption conditions, will be essential for developing design strategies toward functional molecular spintronic architectures.

MATERIALS AND METHODS

Time-resolved magneto-optical Kerr measurements

The sample is mounted in a magneto-cryostat with the external magnetic field **H** approximately perpendicular to the Co-molecular thin-film heterostructure as shown in Fig. 1A. An ultrafast laser pump pulse ($\tau_p < 60$ fs and photon-energy $\hbar\omega = 3.1$ or 1.55 eV) excites the system, inducing a rapid change of the effective anisotropy field from the thermal equilibrium value, $\mathbf{H}_a$, to a perturbed value, $\mathbf{H}'_a$, where both can be statically affected by the external field, **H**. As a result, the magnetization, **M**, starts to coherently precess around the perturbed equilibrium position while losing the unaligned angular momentum component by interactions with the system's electronic and lattice excitations (*16*). The magnetization dynamics is probed using a probe laser pulse (photon-energy $\hbar\omega = 1.55$ eV, within the optical gaps of all the studied molecules) with a variable time delay with respect to the pump pulse. This dynamics is related to the one observed in the FMR experiments, and the spin-wave oscillation frequency, ν, is expected to depend on the

anisotropy field of the system (*16*, *17*). This means that this experimental configuration can be used to extract information about the magnetic anisotropy due to the presence of the interfacial FM-molecular hybridization. To minimize the possible effects of the lateral inhomogeneity, the probe laser beam diameter (~50 μm) was kept slightly smaller than the pump laser beam diameter (~70 μm).

Heterostructure fabrication and characterization

For the two-layer heterostructures, thin Co films (5 nm) were deposited by electron beam (e-beam) evaporation on Al_2O_3 (0001) substrates at room temperature and base pressure of 1.1×10^{-10} mbar with the deposition rate of 0.03 Å/s. The organic layer or the Al layer was subsequently deposited on top of the Co layer by thermal evaporation (base pressure: 1.1×10^{-9} mbar) at room temperature without breaking vacuum. The deposition rates were 0.15 Å/s for C_{60}, 0.25 Å/s for Gaq_3, and 0.1 Å/s for Al.

The four-layer thin-film structures were grown on 0.5-mm-thick (0001) Al_2O_3 substrates. The (111) textured Pt layers of ~4-nm thickness were grown at 500°C by means of e-beam evaporation at a growth rate of ~0.1 Å/s. The substrate was then cooled down to room temperature, and the Co layer (5 nm) was grown also with the e-beam evaporation technique at a rate of ~0.1 Å/s. Within the same chamber, organic molecule layers were sublimed onto the Co surface at a pressure of 5×10^{-10} mbar with a rate of ~0.3 Å/s until a thickness of 20 nm was measured through a quartz monitor. The Cu cap layer (5 nm) was magnetron sputtered on top of the thin-film structure. The heterostructures were then structurally characterized by means of x-ray reflectivity and Raman spectroscopy.

Supplementary Materials

This PDF file includes:

Supplementary Text
Figs. S1 to S9
Table S1
References

REFERENCES AND NOTES

1. M. Cinchetti, V. A. Dediu, L. E. Hueso, Activating the molecular spinterface. *Nat. Mater.* **16**, 507–515 (2017).
2. K. V. Raman, A. M. Kamerbeek, A. Mukherjee, N. Atodiresei, T. K. Sen, P. Lazić, V. Caciuc, R. Michel, D. Stalke, S. K. Mandal, S. Blügel, M. Münzenberg, J. S. Moodera, Interface-engineered templates for molecular spin memory devices. *Nature* **493**, 509–513 (2013).
3. T. Moorsom, M. Wheeler, T. Mohd Khan, F. Al Ma'Mari, C. Kinane, S. Langridge, D. Ciudad, A. Bedoya-Pinto, L. Hueso, G. Teobaldi, V. K. Lazarov, D. Gilks, G. Burnell, B. J. Hickey, O. Cespedes, Spin-polarized electron transfer in ferromagnet/C_{60} interfaces. *Phys. Rev. B* **90**, 125311 (2014).
4. K. Bairagi, A. Bellec, V. Repain, C. Chacon, Y. Girard, Y. Garreau, J. Lagoute, S. Rousset, R. Breitwieser, Y.-C. Hu, Y. C. Chao, W. W. Pai, D. Li, A. Smogunov, C. Barreteau, Tuning the magnetic anisotropy at a molecule-metal interface. *Phys. Rev. Lett.* **114**, 247203 (2015).
5. M. Gruber, F. Ibrahim, S. Boukari, H. Isshiki, L. Joly, M. Peter, M. Studniarek, V. Da Costa, H. Jabbar, V. Davesne, U. Halisdemir, J. Chen, J. Arabski, E. Otero, F. Choueikani, K. Chen, P. Ohresser, W. Wulfhekel, F. Scheurer, W. Weber, M. Alouani, E. Beaurepaire, M. Bowen, Exchange bias and room-temperature magnetic order in molecular layers. *Nat. Mater.* **14**, 981–984 (2015).
6. F. Djeghloul, M. Gruber, E. Urbain, D. Xenioti, L. Joly, S. Boukari, J. Arabski, H. Bulou, F. Scheurer, F. Bertran, P. Le Fèvre, A. Taleb-Ibrahimi, W. Wulfhekel, G. Garreau, S. Hajjar-Garreau, P. Wetzel, M. Alouani, E. Beaurepaire, M. Bowen, W. Weber, High spin polarization at ferromagnetic metal–organic interfaces: A generic property. *J. Phys. Chem. Lett.* **7**, 2310–2315 (2016).
7. T. Moorsom, S. Alghamdi, S. Stansill, E. Poli, G. Teobaldi, M. Beg, H. Fangohr, M. Rogers, Z. Aslam, M. Ali, B. J. Hickey, O. Cespedes, π-Anisotropy: A nanocarbon route to hard magnetism. *Phys. Rev. B* **101**, 060408 (2020).
8. K. Bairagi, A. Bellec, V. Repain, C. Fourmental, C. Chacon, Y. Girard, J. Lagoute, S. Rousset, L. Le Laurent, A. Smogunov, C. Barreteau, Experimental and theoretical investigations of magnetic anisotropy and magnetic hardening at molecule/ferromagnet interfaces. *Phys. Rev. B* **98**, 085432 (2018).
9. S. Boukari, H. Jabbar, F. Schleicher, M. Gruber, G. Avedissian, J. Arabski, V. Da Costa, G. Schmerber, P. Rengasamy, B. Vileno, W. Weber, M. Bowen, E. Beaurepaire, Disentangling magnetic hardening and molecular spin chain contributions to exchange bias in ferromagnet/molecule bilayers. *Nano Lett.* **18**, 4659–4663 (2018).
10. M. Benini, G. Allodi, A. Surpi, A. Riminucci, K.-W. Lin, S. Sanna, V. A. Dediu, I. Bergenti, In-depth NMR investigation of the magnetic hardening in Co thin films induced by the interface with molecular layers. *Adv. Mater. Interfaces* **9**, 2201394 (2022).
11. G. Avedissian, J. Arabski, J. A. Wytko, J. Weiss, V. Papaefthimiou, G. Schmerber, G. Rogez, E. Beaurepaire, C. Meny, Exchange bias at the organic/ferromagnet interface may not be a spinterface effect. *Appl. Phys. Rev.* **9**, 011417 (2022).
12. A. Halder, S. Bhandary, D. D. O'Regan, S. Sanvito, A. Droghetti, Theoretical perspective on the modification of the magnetocrystalline anisotropy at molecule-cobalt interfaces. *Phys. Rev.Mater.* **7**, 064409 (2023).
13. X. Chen, M. Alouani, Effect of metallic surfaces on the electronic structure, magnetism, and transport properties of Co-phthalocyanine molecules. *Phys. Rev. B* **82**, 094443 (2010).
14. M. Benini, A. Shumilin, R. Rakshit, A. Sahoo, A. Halder, A. Droghetti, F. Cugini, M. Solzi, D. Bisero, P. Graziosi, A. Riminucci, I. Bergenti, M. Singh, L. Gnoli, S. Sanna, T. Mertelj, V. Kabanov, S. Sanvito, V. Dediu, The ferromagnetic glass state: Collapse of the standard ferromagnetic domain structure. *Nat Commun* **16**, 5807 (2025).
15. A. Kirilyuk, A. V. Kimel, T. Rasing, Ultrafast optical manipulation of magnetic order. *Rev. Mod. Phys.* **82**, 2731–2784 (2010).
16. M. van Kampen, C. Jozsa, J. T. Kohlhepp, P. LeClair, L. Lagae, W. J. M. de Jonge, B. Koopmans, All-optical probe of coherent spin waves. *Phys. Rev. Lett.* **88**, 227201 (2002).
17. J.-Y. Bigot, M. Vomir, L. Andrade, E. Beaurepaire, Ultrafast magnetization dynamics in ferromagnetic cobalt: The role of the anisotropy. *Chem. Phys.* **318**, 137–146 (2005).
18. Y. Hashimoto, S. Kobayashi, H. Munekata, Photoinduced precession of magnetization in ferromagnetic (Ga,Mn)As. *Phys. Rev. Lett.* **100**, 067202 (2008).
19. E. Carpene, E. Mancini, D. Dazzi, C. Dallera, E. Puppin, S. De Silvestri, Ultrafast three-dimensional magnetization precession and magnetic anisotropy of a photoexcited thin film of iron. *Phys. Rev. B* **81**, 060415 (2010).
20. P. I. Gerevenkov, D. V. Kuntu, I. A. Filatov, L. A. Shelukhin, M. Wang, D. P. Pattnaik, A. W. Rushforth, A. M. Kalashnikova, N. E. Khokhlov, Effect of magnetic anisotropy relaxation on laser-induced magnetization precession in thin galfenol films. *Phys. Rev. Mater.* **5**, 094407 (2021).
21. J. E. Shoup, "Magnetic and structural effects in interfacial magnetism: Molecular magnets and ferrimagnetic alloys," thesis, University of South Florida, FL (2022).
22. C. Chappert, K. L. Dang, P. Beauvillain, H. Hurdequint, D. Renard, Ferromagnetic resonance studies of very thin cobalt films on a gold substrate. *Phys. Rev. B* **34**, 3192–3197 (1986).
23. C. Kittel, Excitation of spin waves in a ferromagnet by a uniform rf field. *Phys. Rev.* **110**, 1295–1297 (1958).
24. P. B. Johnson, R. W. Christy, Optical constants of transition metals: Ti, V, Cr, Mn, Fe, Co, Ni, and Pd. *Phys. Rev. B* **9**, 5056–5070 (1974).
25. J. Stöhr, H. C. Siegmann, *Magnetism: From Fundamentals to Nanoscale Dynamics* (Springer, 2006).
26. S. V. V. Sovskii, *Ferromagnetic Resonance: The Phenomenon of Resonant Absorption of a High-Frequency Magnetic Field in Ferromagnetic Substances* (Elsevier, 2016).
27. J. Jo, J. Byun, I. Oh, J. Park, M.-J. Jin, B.-C. Min, J. Lee, J.-W. Yoo, Molecular tunability of magnetic exchange bias and asymmetrical magnetotransport in metalloporphyrin/Co hybrid bilayers. *ACS Nano* **13**, 894–903 (2019).
28. G. Craig, M. Murrie, 3D single-ion magnets. *Chem. Soc. Rev.* **44**, 2135–2147 (2015).
29. A. K. Bar, C. Pichon, J.-P. Sutter, Magnetic anisotropy in two- to eight-coordinated transition–metal complexes: Recent developments in molecular magnetism. *Coord. Chem. Rev.* **308**, 346–380 (2016).
30. A. Droghetti, S. Steil, N. Großmann, N. Haag, H. Zhang, M. Willis, W. P. Gillin, A. J. Drew, M. Aeschlimann, S. Sanvito, M. Cinchetti, Electronic and magnetic properties of the interface between metal-quinoline molecules and cobalt. *Phys. Rev. B* **89**, 094412 (2014).
31. C. A. Brondin, S. Ghosh, S. Debnath, F. Genuzio, P. Genoni, M. Jugovac, S. Bonetti, N. Binggeli, N. Stojić, A. Locatelli, T. O. Menteş, Tailoring magnetic anisotropy in ultrathin cobalt by surface carbon chemistry. *Adv. Electron. Mater.* **10**, 2300579 (2024).
32. C. Thomsen, H. T. Grahn, H. J. Maris, J. Tauc, Picosecond interferometric technique for study of phonons in the brillouin frequency range. *Optics Commun.* **60**, 55–58 (1986).
33. P. E. Wigen, C. F. Kooi, M. R. Shanabarger, T. D. Rossing, Dynamic pinning in thin-film spin-wave resonance. *Phys. Rev. Lett.* **9**, 206–208 (1962), 10.1103/PhysRevLett.9.206.
34. P. Lubitz, J. J. Krebs, M. M. Miller, S. Cheng, Temperature dependence of ferromagnetic resonance as induced by NiO pinning layers. *J. Appl. Phys.* **83**, 6819–6821 (1998).
35. F. Radu, M. Etzkorn, T. Schmitte, R. Siebrecht, A. Schreyer, K. Westerholt, H. Zabel, Asymmetric magnetization reversal on exchange biased CoO/Co bilayers. *J. Magn. Magn. Mater.* **240**, 251–253 (2002).

36. S. Brems, K. Temst, C. Van Haesendonck, Origin of the training effect and asymmetry of the magnetization in polycrystalline exchange bias systems. *Phys. Rev. Lett.* **99**, 067201 (2007).
37. M. Benini, "Fabrication and characterization of hybrid ferromagnetic-organic heterostructures for spintronics application," thesis, Alma Mater Studiorum, Università di Bologna (2022).

Acknowledgments
Funding: We acknowledge the financial support of the EC project INTERFAST (H2020-FET-OPEN-965046). J.S. acknowledges the Slovenian Research and Innovation Agency young researcher funding no. PR-12840. A.V.S. acknowledges financial support from the European Union (ERC-2021-StG-101042680 2D-SMARTiES). Some calculations were performed on the HAWK cluster of the 2D Smart Materials Lab hosted by the Servei d'Informática of the University of València. T.M. and V.A.D. acknowledge support within the Cooperation Programme on Scientific Cooperation between the National Research Council of Italy and the Jožef Stefan Institute. **Author contributions:** T.M., V.A.D., and M.C. developed the hypothesis and coordinated the experiment. V.A.D. and O.C. defined the heterostructures and coordinated their fabrication. M.B., R.K.R., M.D.R., and S.O. fabricated and characterized the heterostructures. J.S., H.Z., G.J., U.P., and M.B. conducted the TR-MOKE experiments. J.S. and T.M. analyzed the TR-MOKE data. J.S., A.V.S., V.V.K., and T.M. contributed to modeling. All authors contributed to the interpretation of the data. T.M. wrote the paper with input from all authors. **Competing interests:** The authors declare that they have no competing interests. **Data and materials availability:** All data needed to evaluate the conclusions in the paper are present in the paper and/or the Supplementary Materials.

Submitted 24 January 2025
Accepted 1 July 2025
Published 1 August 2025
10.1126/sciadv.adw2243